Rhenium-functionalized covalent organic framework photocatalyst for efficient CO2 reduction under visible light

Shu-Ying Li, Shuang Meng, Xiaoqin Zou, Mohamad El-Roz, Igor Telegeev, Oumaima Thili, Terence Xiaoteng Liu, Guangshan Zhu

Rhenium-Functionalized Covalent Organic Framework Photocatalyst for Efficient CO_2 Reduction under Visible Light

Shu-Ying Li,[#a] Shuang Meng,[#a] Xiaoqin Zou,*[a] Mohamad El-Roz,*[b] Igor Telegeev,[b] Oumaima Thili,[b] and Guangshan Zhu*[a]

[a] Faculty of Chemistry, Northeast Normal University, Changchun 130024, P. R. China.

[b] Normandie University, Ensicaen, Unicaen, CNRS, Laboratoire Catalyse et Spectrochimie, 14000 Caen, France.

[#] The authors contributed equally to this work.

* Corresponding authors: zouxq100@nenu.edu.cn (X. Q. Zou), mohamad.elroz@ensicaen.fr (M. El-Roz), zhugs100@nenu.edu.cn (G. S. Zhu).

Abstract

The conversion of carbon dioxide (CO_2) into value-added chemicals under photochemical conditions has attracted increasing attention in recent years. One of the great challenges is to develop novel visible catalysts with sustained lifetime and high activity. In this regard, herein, we report a highly efficient, stable and recyclable photocatalyst by embedding photoactive rhenium complex ($Re(CO)_5Cl$) into porous, crystalline, bipyridine-based covalent organic frameworks (COFs). The rhenium post-metallated COFs exhibits salient photocatalytic activity towards CO_2 reduction under visible light. The quantity of the CO produced on Re-functionalized COFs is twice higher than that produced on the famous $Re(bpy)(CO)_3Cl$ (bpy = 2,2'-bipyridine) molecular photocatalyst under similar reaction conditions.

Introduction

Massive CO_2 is released into atmosphere with an increasing use of fossil fuels, which may bring many environmental problems such as global warming. Facilitating the conversion of greenhouse gas CO_2 into valuable chemicals like CO, CH_4, HCOOH, and CH_3OH can tackle the issues of fossil fuel shortage and global warming at once[1-4]. Among numerous approaches for CO_2 transformation, reducing CO_2 by exploiting solar light is regarded as a promising alternative which is economical

and widely available[5-8]. As is known, photocatalysts based on Re^{I} bipyridine complexes [Re^{I}(bpy)$(CO)_3Cl$] have been extensively explored as highly active photocatalysts for consuming CO_2 to produce CO or $HCOO^-$ under visible light[9,10]. However, molecular catalysts usually aggregate together easily during reaction process resulted in catalyst deactivation. In addition, the recycling and reuse of the catalysts from the reaction media is very difficult. Therefore, developing efficient, durable and recyclable photocatalysts for CO_2 reduction is of high importance.

Covalent organic frameworks (COFs) are a new class of porous materials with high crystallinity, large surface area and designable structure, which are attractive in numerous fields such as gas adsorption and separation, catalysis and molecular sensing[11-14]. The skeleton and property of COFs can be tuned by adjusting the symmetry, size and nature of building units[15,16]. Notably, when molecular catalysts are incorporated into topological frameworks, the integration could exhibit more efficient performance than the corresponding molecular catalysts[17]. One intriguing example is that dramatic improvement of catalytic efficiency has been achieved for a polymeric ionic polymer bearing Lewis acid sites rather than its individual components[18]. Furthermore, well-defined COFs are able to provide a uniform catalytic environment which is essential for the investigation of physicochemical mechanism during reaction process. Therefore, it is promising for COFs to serve as host platforms accommodating guest active moieties and to realize cooperative functions[19].

Herein, we demonstrate the synthesis of an efficient photocatalyst with isolated, molecularly defined catalytic sites for CO_2 reduction to CO by loading rhenium complex ($Re(CO)_5Cl$) onto the pore walls of COFs (TpBpy) comprising rich 2,2'-bipyridine groups (Figure 1). The modified COFs (Re-TpBpy) still preserve the crystallinity and have a high surface area, thereby offering a catalytic environment and a ready access for CO_2 to the catalytic sites. Anchoring rhenium complex into COFs not only facilitates a dispersive arrangement of active sites generating enhanced photocatalysis efficiency, but also prevents the losing of active species resulted in a recyclable catalyst with the long-term stability. The present results bring new enlightenments in fabricating well-defined, efficient, recyclable photocatalyst by utilizing highly ordered COFs with available chelating sites as a platform for functional moieties.

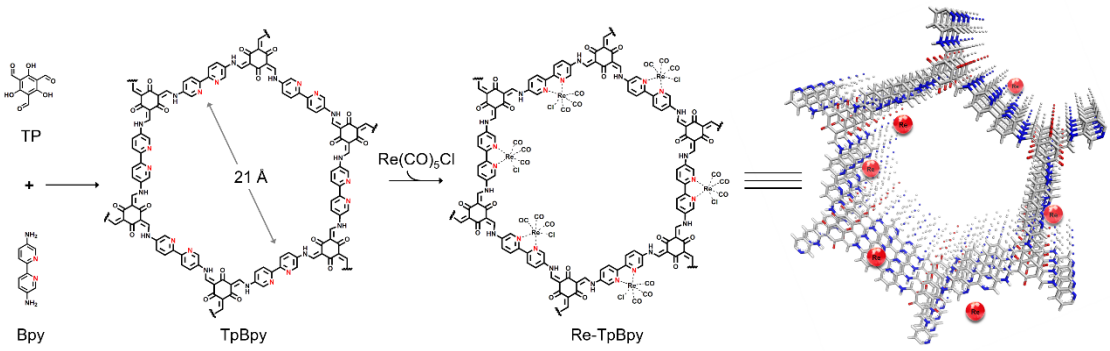

Figure 1. Illustration for the construction steps of TpBpy and Re-TpBpy COFs.

Results and discussion

Characterization of the photocatalyst

The preparation of TpBpy COF is performed by reacting 1, 3, 5-triformylphloroglucinol (Tp) and 2,2'-bipyridine-5,5'-diamine (Bpy) *via* Schiff-base condensation according to a previously reported

protocol[20]. As depicted in Figure 2a, the experimental powder X-ray diffraction (PXRD) results are in accordance with the simulated 2D model based on AA stacking structure in the hexagonal space group (P6/m). The PXRD pattern of Re-TpBpy exhibits an intense first peak at 2θ of 3.6°, corresponding to the reflection from (100) plane. Considering the (001) facet emerging at 25.6°, the π–π stacking interlayer distance in COF is deduced to be 3.5 Å. On the other hand, the rhenium-modified TpBpy (Re-TpBpy) is synthesized by refluxing $Re(CO)_5Cl$ with TpBpy in methanol for 24 h under N_2 atmosphere. The collected PXRD pattern displays the first intense peak at the same position (2θ = 3.6°) as that of TpBpy, which demonstrates the retention of the pristine framework structure of TpBpy COFs after rhenium incorporation.

N_2 adsorption isotherms at 77 K were measured to investigate the porosity of TpBpy and Re-TpBpy COFs (Figure 2b). The surface area of primitive TpBpy COF is 1526 $m^2\ g^{-1}$, whereas Re-TpBpy COF exhibits a decrease in the surface area (632 $m^2\ g^{-1}$). This phenomenon is supposed to be resulted from the occupancy of partial pore spaces in Re-TpBpy COF by $Re(CO)_3Cl$ moieties and to the higher density of the Re-TpBpy in respect to the TpBpy composite. Notably, the BET surface area of Re-TpBpy is still relatively high and the porous structure is well preserved. Therefore, a high accessibility of the Re active sites in the COF channels can be investigated.

Besides, the functionalization of the open N,N'-chelating sites with $Re(CO)_3Cl$ group in as-prepared Re-TpBpy was further verified by Fourier Transform Infrared (FTIR) spectroscopy (Figure 2c). Upon complexation, two additional peaks arise at 2027 and 1903 cm^{-1} in the spectrum of Re-TpBpy relative to the FT-IR peaks of TpBpy, which are assigned to the C=O stretching vibration in $Re(CO)_3Cl$ moiety. Furthermore, in the FT-IR spectrum of Re-TpBpy, the emerged C=O stretching bonds (2027 and 1903 cm^{-1}) and the broadened C-N peak at 1248 cm^{-1} reveal a slight red shift compared with those in the starting material of $Re(CO)_5Cl$ (2043 and 1961 cm^{-1}) and TpBpy COF (1266 cm^{-1}), respectively, indicative of the formation of Re–N bonds between $Re(CO)_3Cl$ complex and 2,2'-bipyridine groups.

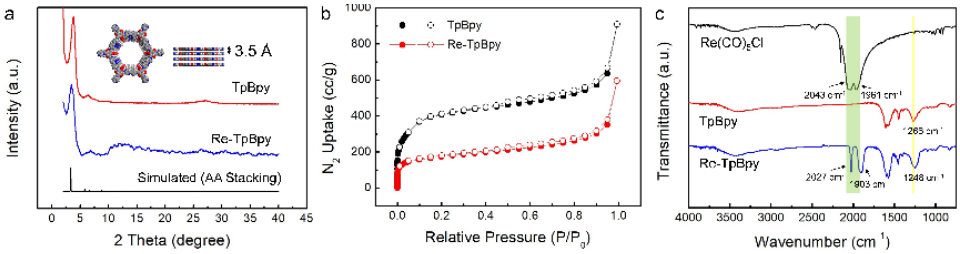

Figure 2. Comparative (a) powder X-ray diffraction (PXRD) patterns, (b) N_2 adsorption-desorption isotherms collected at 77 K, and (c) FT-IR spectra.

To provide additional proof, X-ray photoelectron spectroscopy (XPS) analysis was performed. The two nitrogen species in deconvoluted N 1s spectrum located at 400.19 eV and 398.99 eV are ascribed to the secondary nitrogen and pyridinic nitrogen in TpBpy, respectively (Figure 3b)[21]. After TpBpy functionalization, two sets of signals corresponding to 42.54 eV and 198.22 eV are observed as shown in Figure 3a, which are assigned to rhenium and chlorine, respectively, indicating the existence of rhenium complex in the host COF. It is noteworthy that, upon rhenium impregnation, the binding energy of pyridinic nitrogen shifts to the higher energy position from 398.99 eV to 400.46 eV (Figure 3c), implying the coordination between rhenium and nitrogen in bipyridine. Furthermore, the peak position of secondary nitrogen remains almost unchanged at 400.19 eV,

which indicates that the rhenium complex chelates to bipyridinic units in TpBpy COF only. The total desapearance of the signal at 398.99 demonstrate the high yield of functionalization of the TpBpy with $Re(CO)_3Cl$ group.

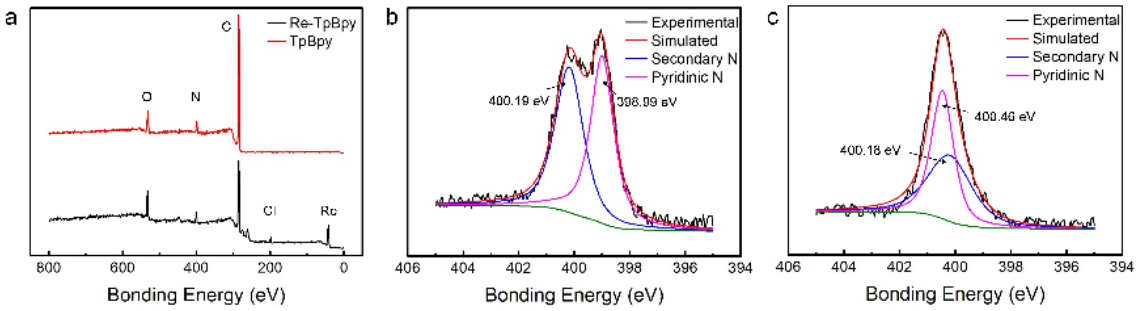

Figure 3. (a) XPS survey of TpBpy and Re-TpBpy COFs, (b) and (c) correspond to the XPS N 1s spectra of TpBpy and Re-TpBpy, respectively.

The quantitative measurement acquired by inductively coupled plasma optical emission spectroscopy (ICP-OES) illustrates that the mass fraction of Re in the prepared Re-TpBpy COF is up to 26.4%. Additionally, transmission electron microscopy (TEM), scanning electron microscopy (SEM) and local energy-dispersive X-ray (EDX) spectra investigations were also carried out to further evaluate the distribution and the status of Rhenium in the Re-TpBpy COF. According to the electron microscopic observation, there is no obvious difference in the morphology could be distinguished between the parent TpBpy and the Re- functionalized TpBpy COFs (Figure S1 in ESI). TEM images in Figure 4a reveal that no metal aggregates are detected in the COF material. Moreover, EDX mapping *via* SEM also demonstrates a homogeneous distribution of Re, N, C and O content in Re-TpBpy (Figure 4b-f), implying an atomically integration of rhenium species into the Re-TpBpy COF.

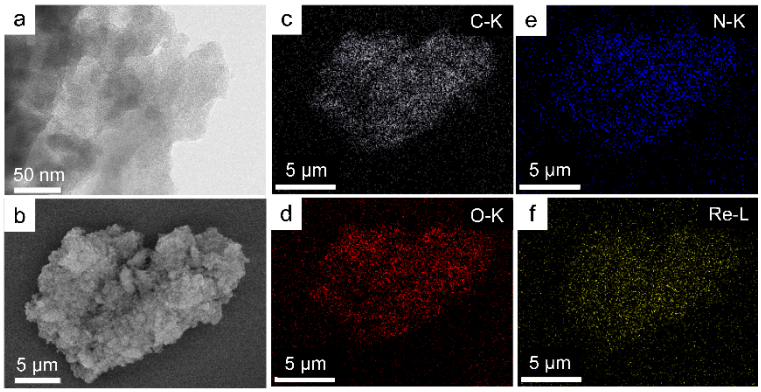

Figure 4. TEM (a) and SEM (b) images, and the elemental mapping of the Re-TpBpy COF (c-f).

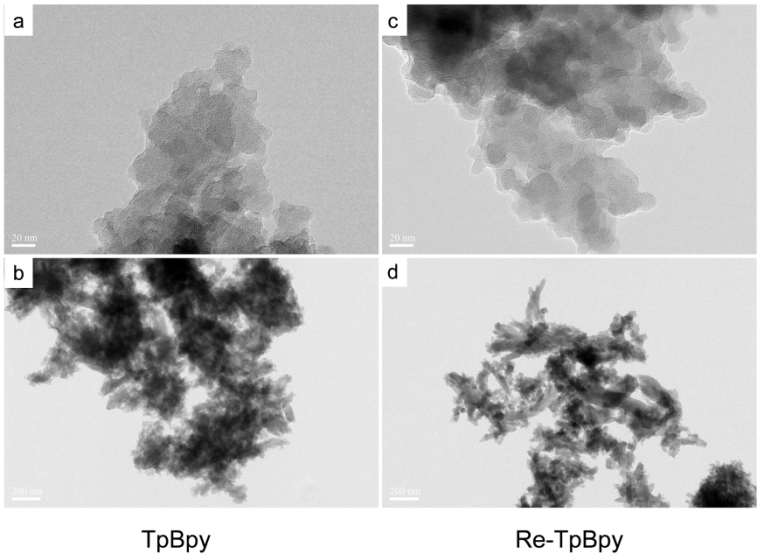

Figure S1. TEM images for (a, b) TpBpy and (c, d) Re-TpBpy COFs.

Table S1. Results from N_2 adsorption-desorption measurements.

Sample	S_{BET}	Pore Diameter	Pore Volume
TpBpy	1526 $m^2 g^{-1}$	2.05 nm	1.10 cc g^{-1}
Re-TpBpy	632 $m^2 g^{-1}$	1.67 nm	0.67 cc g^{-1}

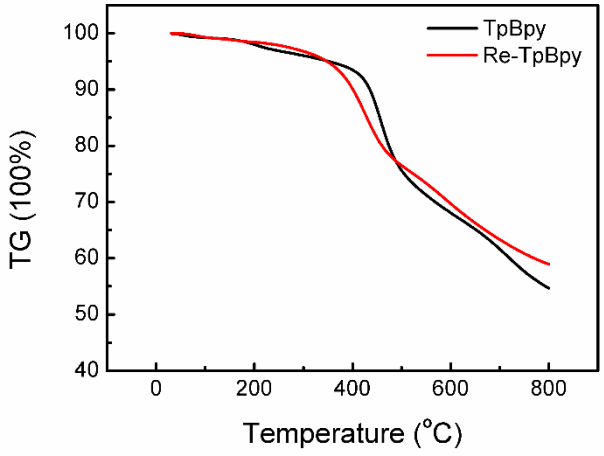

Figure S2. TGA profiles of TpBpy and Re-TpBpy COFs in N_2 atmosphere.

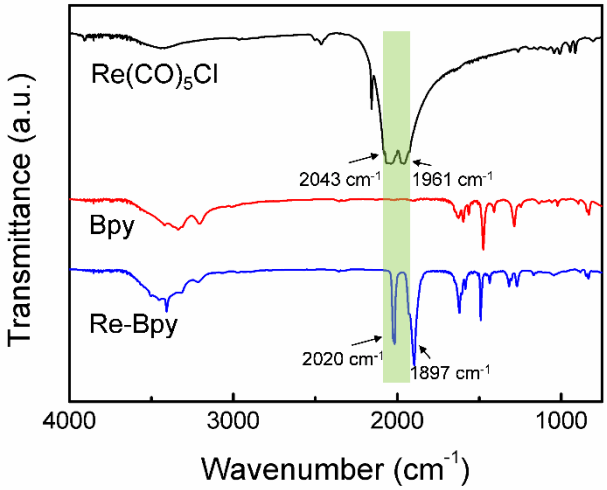

Figure S3. FT-IR spectra of Bpy, Re-Bpy and $Re(CO)_5Cl$.

Since the 2, 2'-bpy fragment in the TpBpy COF is the essential part for coordination with $Re(CO)_5Cl$, the reference compound $Re(bpy)(CO)_3Cl$ (bpy = 2,2'-bipyridine) (abbreviated as Re-Bpy) was also synthesized to explore the photocatalytic mechanism in CO_2 reduction. FTIR spectrum and XPS characteristics of Re-Bpy can be found in ESI. ICP-OES results indicate the mass fraction of Re in the prepared Re-Bpy is about 32%.

As is known, the adsorption of CO_2 onto catalyst surface is prerequisite for the following catalytic process. Porous structure in the Re-TpBpy COF may facilitate the capture of CO_2 and play a critical role in promoting the conversion of CO_2. As depicted in Figure 5, Re-TpBpy COF displays a CO_2 adsorption volume of 44 $cm^3\ g^{-1}$ at atmospheric pressure at 298 K while the CO_2 adsorption capability of Re-Bpy is almost zero. Additionally, the steeper uptake for CO_2 at low relative pressures is observed in the Re-TpBpy COF compared to that of TpBpy COF, implying a stronger interaction of CO_2 in Re-TpBpy. Both results of higher adsorption volume and stronger interaction enable the Re-TpBpy COF to serve as a more promising photocatalyst for CO_2 reduction. It should be noted that in a solid/liquid phase heterogeneous reaction, the porosity of the catalyst can play a crucial role on the activity of the catalyst by insuring a high catalyst/reactant contact time. However, for the homogeneous catalytic reactoion (case of Re-Bpy), the reaction is diffusional and it is not related with the adsorbate capacity of the catalyst. Therefore, contact time between the CO_2 and the Re active site is higher in the case of Re-Bpy catalyst than that in Re-TpBpy catalyst.

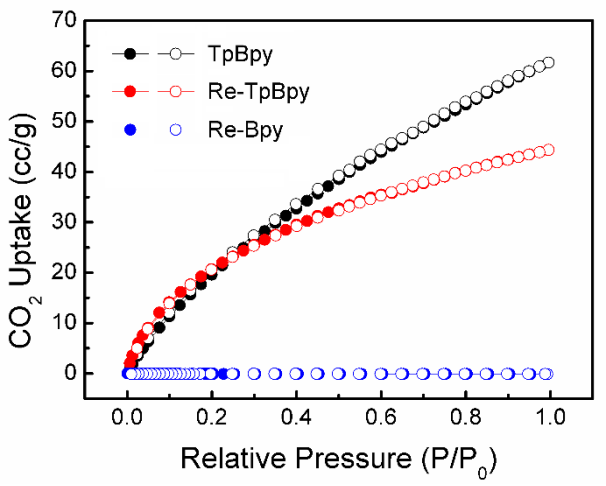

Figure 5. CO_2 uptakes on TpBpy and Re-TpBpy COFs, and the Re-Bpy molecular compound at 298 K; P_0 here refers to 1.0 bar.

The DR-UV-visible spectra of the different samples are presented in Figure 6. A clear enhancement of the visible light absorbance of Re-TpBpy in respect to Re-Bpy can be observed. This is due to the increase of the electron conjugation/delocalization of the COF framework of Re-TpBpy. On the other hand, both TpBpy and Re-TpBpy materials show similar light absorbance behavior, demonstrating the high stability of the ligand (chromophore function) after functionalization. However, a higher absorbance of the visible light can't warranty a higher photocatalytic performance. Only the photocatalytic tests can confirm or not the performance enhancement of the photocatalyst under visible light irradiation.

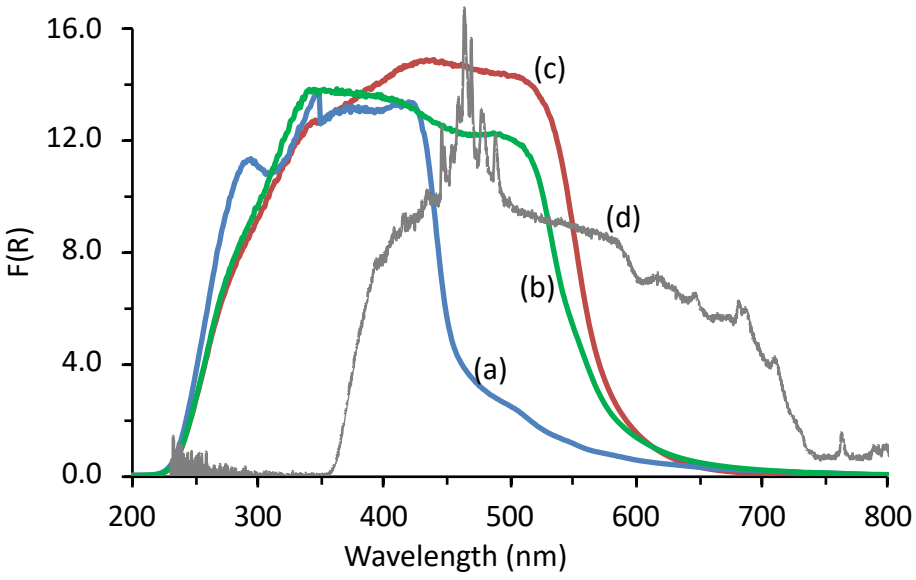

Figure 6. DR-UV-visible spectra of Re-Bpy (a), TpBpy (b), and Re-TpBpy (c) samples studied in this work. (d) corresponds to the emission spectrum of the Xe-lamp (with pass-high filter at 390 nm) used in the photocatalytic test.

Photocatalytic CO_2 reduction

The CO_2 photoreduction was performed using a new *in-situ* FTIR reactor (in a batch mode) as described in the experimental section. More details about the reactor can be found in reference x. The photocatalysts have been tested under similar reaction condition used in the literature. Re-TpBpy, Re-Bpy and TpBpy compounds were first dispersed in acetonitrile and water solution contained triethanolamine as electron donor. The solutions were then purged by Argon, in order to ensure an oxygen free atmosphere, and then with $^{12}CO_2$ or $^{13}CO_2$. The catalysts was then tested under similar reaction conditions using Xe-lamp with a pass high filter (>390nm) as visible light source. The CO production in the reaction headspace was followed by in-situ FTIR analysis using the IR band intensity of the characteristic CO vibrations at 2200-2100 cm^{-1} (insert figure 6). The results of CO production during photocatalytic CO_2 reduction on the different materials are displayed in Figure 6. No CO is detected by using TpBpy materials. This expected result shows that the ligand is not producing CO (by degradation) even after long irradiation time (16 h).

Re-Bpy and Re-TpBpy photocatalyst are both active under visible light and similar efficiency can be observed in the first hours of irradiation. After four hours of the reaction, a deviation on the CO production can be observed. The quantity of the CO produced on Re-TpBpy is twice higher than that produced on the Re-Bpy photocatalyst after 12 h of irradiation. As the reaction is realized in the liquid phase, the accessibility of the CO_2 toward the active site is higher in the molecular photocatalyst (Re-Bpy) than that in case of Re-TPBpy. This behavior can compensate the higher visible light absorbance of Re-TpBpy and justify the similar activity in the first hour of irradiation. However, the higher decline of the activity of the Re-Bpy catalyst can probably assigned to its relatively low stability in respect to Re-TpBy. This stability was confirmed by a second cycle of the Re-TpBpy catalyst. The decrease of the activity after the second cycle is low than 20% as demonstrate the analysis of the gas headspace of the reaction using the gas chromatography (Figure 7), in agreement with the results obtained by in-situ FTIR analysis. It should be noted that no activity was observed under inert atmosphere (Ar) for Re-TpBpy, Re-Bpy and TpBpy.

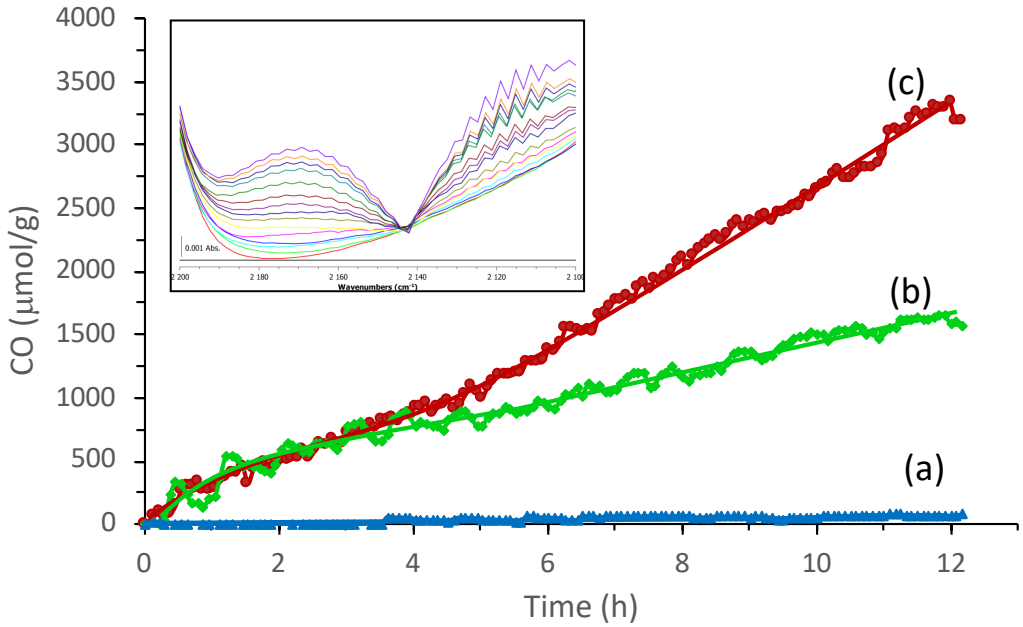

Figure 6. Time course of CO production during photocatalytic CO_2 reduction on TpBpy, Re-Bpy and Re-TpBpy photocatalyst under visible light irradiation. Insert: evolution of the CO vibration band during the CO_2 reduction on Re-TpBpy (time resolution 1 h/spectrum). Condition: irradiation wavelength>390nm; Irradiance= 205 mW/cm^2; catalysts concentration=1mM in AcN/H_2O mixture (10 ml:1.8 ml); 0.1 M of TEOA.

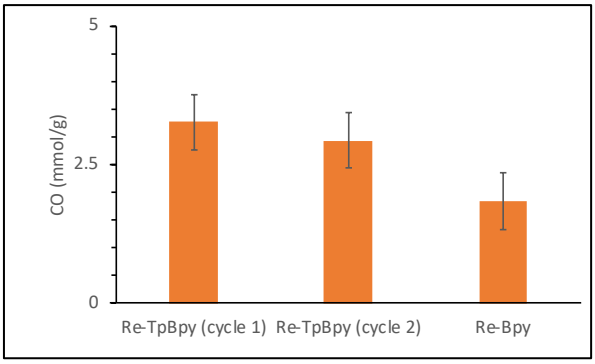

Figure 7. CO produced during the CO_2 photoreduction on Re-TpBpy and Re-Bpy photocatalysts as determined by in-situ FTIR and GC analysis of the gas products of the reaction headspace. Reaction performed in AcN/H_2O (10/1.8 ml/ml) in presence of triethanolamine (0.1 M) and 15 mg of photocatalyst under 12h of visible light irradiation (l>390nm; irradiance = 205 mW/cm^2).

For confirming the origin of the CO production, the experiment of the CO2 reduction on Re-TpBpy was repeated by using ^{13}C labeled CO_2 under the same condition used above. The FTIR analysis of the gas phase reveals the selective formation of only labeled ^{13}CO after 12h of irradiation (Figure 8). There is no formation $^{12}CO_2$ which exclude the total oxidation reactions of the ligand and/or the electron donor.

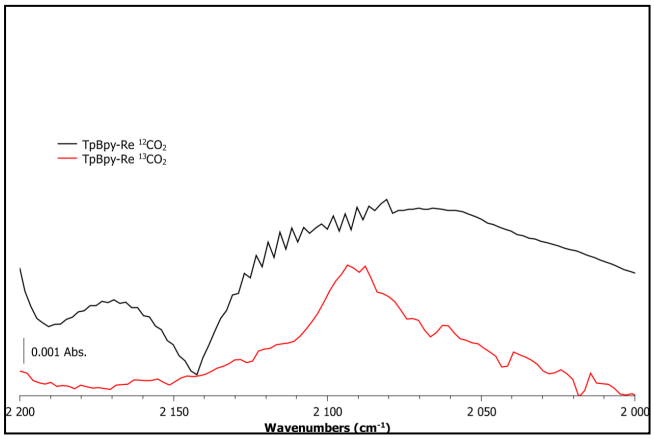

Figure X4. FTIR spectra of the reaction headspace in the CO vibration range after $^{12}CO_2$ (black) and $^{13}CO_2$ (red) photoreduction using Re-TpBpy as photocatalyst. Reaction performed in AcN/H_2O (10/1.8 ml/ml) in presence of triethanolamine (0.1 M) and 15 mg of photocatalyst under 12h of visible light irradiation (l>390nm; irradiance = 205 mW/cm^2).

In summary, the photocatalyst tests demonstrate clearly the advantages of the new recyclable Re-TpBpy photocatalyst synthesized in this work for the selective CO_2 reduction under visible light irradiation.

Conclusions

A rhenium-functionalized COF (Re-TpBpy) was developed to serve as a recyclable catalyst with durable and high activity for photocatalytic reduction of CO_2 to CO. Bipyridine groups in the COF channels furnished uniform coordination sites for the chelation with metal complex, generating isolated and molecularly defined catalytic sites on the pore walls of Re-TpBpy. Experimental results revealed that the Re-TpBpy photocatalyst exhibited two times more active than the reference compound (Re-Bpy) under the same reaction condition, and a constant increase of CO amount was observed even after 16 h of irradiation. Immobilization of metallic active center into highly-ordered COFs is proposed to be a promising approach towards CO_2 conversion, which not only promotes photocatalysis efficiency but also prevents the losing of active species.

Experimental Section

Physical measurements

FTIR spectra (KBr) were recorded on Nicolet IS50 Fourier transforms infrared spectrometer. N_2 adsorption-desorption isotherms and pore size distributions were obtained at 77 K using an Autosorb iQ2 adsorptometer, Quantachrome Instrument. CO_2 adsorption isotherms were obtained on the same apparatus at 298 K. PXRD measurements were performed on Rigaku D/MAX2550 diffractometer using Cu-Kα (λ = 1.5418 Å) radiation running at a voltage of 40 kV and a current of 200 mA. TEM images were measured on JEOL JEM 3010. SEM imaging was implemented on field emission scanning electron microscope equipped with energy-dispersive X-ray spectroscopy (FE-SEM, SU-

8010, Hitachi). The X-ray photoelectron spectroscopy (XPS) spectra were collected on a Thermo ESCALAB 250 instrument using Al-Kα as the exciting radiation (energy step size of 1.0 eV, pass energy of 20.0 eV) and binding energy calibration was based on C 1s at 284.6 eV. Metal contents in the COF were measured by ICP-OES on a ThermoScientificiCAP6300. The Thermo Gravimetric Analysis (TGA) experiments were conducted on the Perkin Elmer thermogravimetric analyzer at a heating rate of 10 °C min^{-1} in N_2 atmosphere.

Synthesis of TpBpy COF

All starting solid chemicals and solvents were obtained commercially and used without further purification. TpBpy COF was synthesized following a previous literature. In brief, 1,3,5-triformylphloroglucinol (Tp) (25.2 mg) and 2,2'-bipyridine-5,5'-diamine (Bpy) (33.5 mg) were added into a pyrex tube (o.d. × i.d. = 16 × 12 mm^2 and length 18 cm) and dissolved in the mixture of 1.8 mL of dimethylacetamide (DMAc), 0.6 mL of o-dichlorobenzene (o-DCB) and 0.24 mL of 6.0 M aqueous acetic acid (AcOH). This reaction mixture was sonicated for 15 minutes to obtain a homogenous dispersion. The tube was flash-frozen in a liquid N_2 bath (77 K), degassed by three freeze-pump-thaw cycles and flame sealed. Then the mixture was heated at 120 °C and left undisturbed for 3 days, yielding a dark-red solid. Then the tube was broken at neck. The product was isolated by filtration and washed with DMAc, water and acetone. The collected powder was immersed in acetone for 12 h, during which the activation solvent was replenished three times. Finally, the product was dried at 100 ºC under vacuum for 24 h to afford TpBpy COF in 75% isolated yield.

Synthesis of Re-TpBpy COF

TpBpy COF (35 mg) and $Re(CO)_5Cl$ (47.9 mg) were mixed in 10 mL methanol (MeOH). The mixture was then refluxed for 24 h under N_2. The resultant red powder was washed with MeOH three times and collected by vacuum filtration. Finally, the product was dried at 80 ℃ in vacuum for 12 h.

Synthesis of Re-Bpy Molecular Compound

Bpy (19 mg) and $Re(CO)_5Cl$ (36.2 mg) were mixed in 10 mL methanol (MeOH). The mixture was then refluxed for 24 h under N_2. The resultant yellow powder was washed with MeOH three times and collected by vacuum filtration. Finally, the product was dried at 80 ℃ in vacuum for 12 h.

Photocatalytic Measurements

The photocatalytic CO_2 reduction was tested in a new in-situ reactor developed recently in the LCS laboratory and presented in Scheme X1.(ref) The reactor is made from glass and equipped with two gas inlet and outlet, perpendicular to the tubes ensuring the FTIR beam pathway through CaF_2 windows. The FTIR tubes are slightly tilted to prevent the solvent condensation and accumulation. The UV-visible irradiation is ensured from the top through a removable quartz window. The quartz and CaF_2 widows are attached to the reactor with screw fittings and the tightness is obtained by adapted Teflon O-rings. The total internal volume of the reactor is 160 ± 5 ml and can be filled with 10 to 50 ml of the solution. The design allowed an easy opening and closing of the reactor, therefore, an easy clean after each experiment. The purge of the reactor is ensured by the mass flow controller system. All IR spectrum measurements with the *in situ* FTIR reactor were monitored in real time

with 2 to 5 min/spectrum of time resolution. IR spectra of the reactor headspace were recorded using Nicolet 6700 IR spectrometer (Thermo Fisher Scientific) equipped with an MCT detector. All photocatalytic tests presented in this work were performed in batch configuration and at room temperature (25-30°C). As a light source, Xe-lamp (LC8 Hamamatsu, 200 W) with pass-high filter at 390 nm was used. 1 mM of the photocatalysts has been dispersed in AcN/H_2O mixture (10/1.8 ml) contained 0.1 M of triethylamine (TEOA) as electron donor. The solution was sonicated for 30 min at room temperature and bubbled with argon and then with CO_2 for 30 min with a flow rate of 20 mL/min.

Off-line GC analysis of CO were conducted using Thermo Scientific Trace 1310 with a Thermal conductivity detector (GC-TCD for TRACE 1300 GC Series, Thermo Scientific), and equipped with a MolSive5 A column (30 m × 0.53 mm, 50 µm). For this purpose, injections (1 ml) of gas headspace were made in the GC and the resulting peak areas were converted into concentrations by using a calibration with the corresponding standard gas (operating conditions: carrier gas: He; split flow rate = 60 mL/min; split ratio= 1/12; inlet temperature = 423 K; column temperature 393 K.

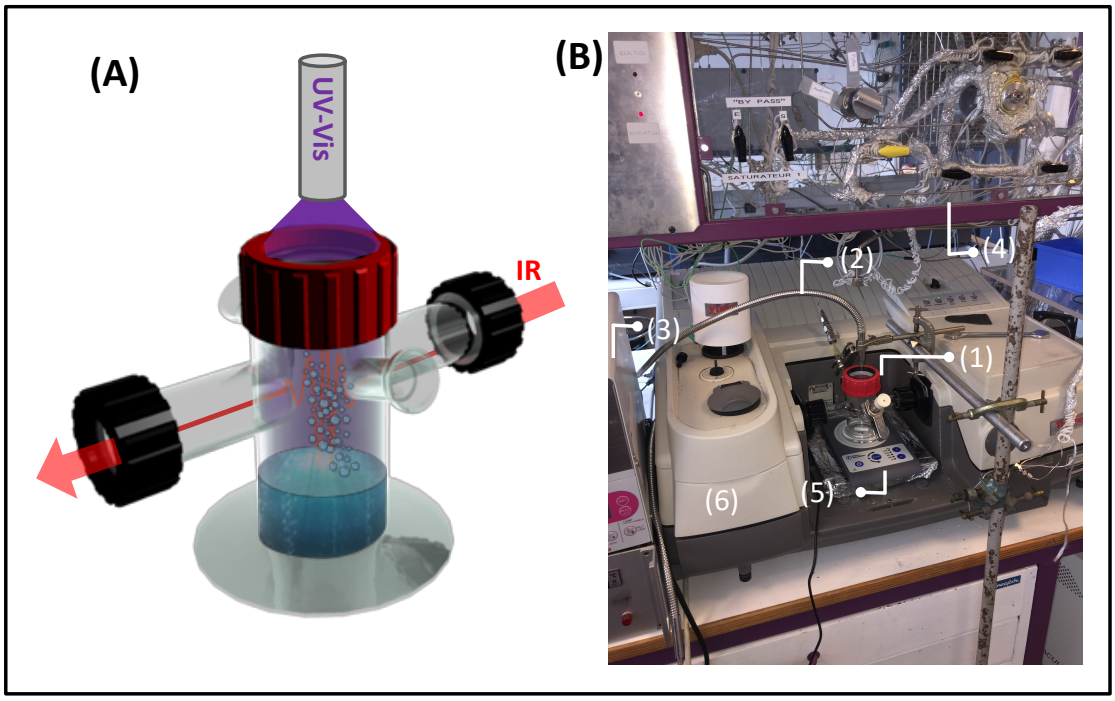

Scheme X1. (A) the in situ FTIR reactor and (B) the entire setup used for performing the photocatalytic tests: (1) in-situ FTIR reactor; (2) optical fiber guidelight; ; (3) Light source; (4) Gas flow setup (for purge); (5) Magnetic steerer; (6) FTIR spectrometer. More details on the setup can be found in reference X.

References

(1) Lin, S.; Diercks, C. S.; Zhang, Y.-B.; Kornienko, N.; Nichols, E. M.; Zhao, Y.; Paris, A. R.; Kim, D.; Yang, P.; Yaghi, O. M.; Chang, C. J. *Science* **2015**, *349*, 1208.

(2) Waki, M.; Yamanaka, K.-i.; Shirai, S.; Maegawa, Y.; Goto, Y.; Yamada, Y.; Inagaki, S. *Chemistry – A European Journal* **2018**, *24*, 3846.

(3) Tu, W.; Zhou, Y.; Zou, Z. *Advanced Materials* **2014**, *26*, 4607.

(4) Liu, X.; Inagaki, S.; Gong, J. *Angewandte Chemie International Edition* **2016**, *55*, 14924.

(5) Morris, A. J.; Meyer, G. J.; Fujita, E. *Accounts of Chemical Research* **2009**, *42*, 1983.

(6) Huang, R.; Peng, Y.; Wang, C.; Shi, Z.; Lin, W. *European Journal of Inorganic Chemistry* **2016**, *2016*, 4358.

(7) Koike, K.; Grills, D. C.; Tamaki, Y.; Fujita, E.; Okubo, K.; Yamazaki, Y.; Saigo, M.; Mukuta, T.; Onda, K.; Ishitani, O. *Chemical Science* **2018**, *9*, 2961.

(8) Deng, X.; Albero, J.; Xu, L.; García, H.; Li, Z. *Inorganic Chemistry* **2018**, *57*, 8276.

(9) Xu, R.; Wang, X.-S.; Zhao, H.; Lin, H.; Huang, Y.-B.; Cao, R. *Catalysis Science & Technology* **2018**, *8*, 2224.

(10) Takeda, H.; Koike, K.; Inoue, H.; Ishitani, O. *Journal of the American Chemical Society* **2008**, *130*, 2023.

(11) Liao, H.; Wang, H.; Ding, H.; Meng, X.; Xu, H.; Wang, B.; Ai, X.; Wang, C. *J. Mater. Chem. A,* **2016**, *4*, 7416.

(12) Segura, J. L.; Mancheno, M. J.; Zamora, F. *Chem. Soc. Rev.* **2016**, *45*, 5635.

(13) Lu, Q.; Ma, Y.; Li, H.; Guan, X.; Yusran, Y.; Xue, M.; Fang, Q.; Yan, Y.; Qiu, S.; Valtchev, V. *Angewandte Chemie International Edition* **2018**, *57*, 6042.

(14) Han, X.; Xia, Q. C.; Huang, J. J.; Liu, Y.; Tan, C. X.; Cui, Y. *J. Am. Chem. Soc.* **2017**, *139*, 8693.

(15) Ding, S.-Y.; Wang, W. *Chemical Society Reviews* **2013**, *42*, 548.

(16) Huang, N.; Wang, P.; Jiang, D. L. *Nat. Rev. Mater.* **2016**, *1*, 16068.

(17) Wang, C.; Xie, Z.; deKrafft, K. E.; Lin, W. *Journal of the American Chemical Society* **2011**, *133*, 13445.

(18) Sun, Q.; Aguila, B.; Perman, J.; Nguyen, N.; Ma, S. *Journal of the American Chemical Society* **2016**, *138*, 15790.

(19) Blake, A. J.; Champness, N. R.; Easun, T. L.; Allan, D. R.; Nowell, H.; George, M. W.; Jia, J.; Sun, X.-Z. *Nature Chemistry* **2010**, *2*, 688.

(20) Shinde, D. B.; Aiyappa, H. B.; Bhadra, M.; Biswal, B. P.; Wadge, P.; Kandambeth, S.; Garai, B.; Kundu, T.; Kurungot, S.; Banerjee, R. *Journal of Materials Chemistry A* **2016**, *4*, 2682.

(21) Elko-Hansen, T. D. M.; Ekerdt, J. G. *Chemistry of Materials* **2014**, *26*, 2642.

TOC